Modeling the diurnal cycle over tropical oceans using the weak temperature gradient approximation

Sharon L. Sessions, * Leah A. Lindsey,

Carlos López Carrillo, and David J. Raymond

Physics Department and Geophysical Research Center,

New Mexico Institute of Mining and Technology, Socorro, NM 87801

* *Corresponding author address:* Sharon L. Sessions, Department of Physics and Geophysical Research Center, New Mexico Institute of Mining and Technology, 801 Leroy Pl., Socorro, NM 87801.

E-mail: sessions@kestrel.nmt.edu

ABSTRACT

We investigate the extent to which precipitation over tropical oceans is modulated by the diurnal variations in the thermodynamic environment. Tropical precipitation is modeled using a cloud system resolving model with the large scale parameterized using the weak temperature gradient (WTG) approximation. In WTG, convection responds to specified potential temperature and humidity profiles. By imposing diurnal variations observed during the 2001 EPIC field program to the reference profiles of potential temperature and mixing ratio, we assess the extent to which convection responds to these changes and accounts for the diurnal variability in precipitation observed during EPIC. Remarkably, the WTG approximation is able to reproduce a precipitation maximum near the observed time, despite an imperfect reproduction of the diurnal variability in saturation fraction. The ability of the model to capture the diurnal variability relies heavily on a strict enforcement of the WTG approximation and the lateral entrainment of moisture into the model domain resulting from this enforcement.

1. Introduction

Understanding the diurnal variability in precipitation over tropical oceans remains an important and difficult problem. Observations show that the diurnal amplitude over oceans is weak compared to that over land, and that the peak in precipitation occurs in the early morning hours with a weaker afternoon peak in some ocean regions (Yang and Slingo 2001; Nesbitt and Zipser 2003). The weak afternoon peak is associated with an increase in absorption of shortwave radiation, either by the ocean surface (Chen and Houze 1997; Sui et al. 1997) or by clear sky water vapor (Takahashi 2012). It is often obliterated in disturbed environmental conditions, and is therefore only present in limited observations where afternoon convection is associated with small, unorganized systems (Nesbitt and Zipser 2003; Cifelli et al. 2008).

The origin of the predominant early-morning precipitation maximum is not as well understood. For ocean regions in the vicinity of land, there is a strong influence from the diurnal heating of the land itself. The land-based diurnal forcing may result from extended sea breezes (Gille et al. 2003; Takahashi 2012), or from longer-ranged propagation of gravity waves initiated from land-based convection (Mapes et al. 2003a,b; Warner et al. 2003; Yang and Slingo 2001; Jiang 2012).

Ocean regions which are far from land influence also exhibit an early morning rainfall maximum. The popular mechanisms explaining this peak all involve the interaction between radiation and convection. Some mechanisms suggest that convection increases as a result of thermal destabilization of upper clouds due to enhanced radiative cooling of cloud tops (Kraus 1963; Ramage 1971; Randall et al. 1991); others emphasize the role of cloud-free regions, stating that absorption of solar radiation by water vapor warms the clear-sky regions which inhibits convective growth by reducing convergence into cloudy regions during the day (Ruprect and Gray 1976a,b; Gray and Jacobson 1977). At least one numerical study concluded that the direct interaction between radiation and convection played the primary role in modulating diurnal precipitation, with the interaction between cloudy and cloud-free regions playing a secondary role (Liu and Moncrieff 1998).

The timing and prominence of the rainfall maximum is influenced further by interactions with large-scale tropical waves (Chen and Houze 1997; Sui et al. 1997), wind patterns (Pereira and Rutledge 2006; Takahashi 2012), seasonality (Hendon and Woodberry 1993; Biasutti et al. 2012), location (Hendon and Woodberry 1993; Kubota and Nitta 2001; Yang and Slingo 2001; Nesbitt and Zipser 2003; Cifelli et al. 2008; Biasutti et al. 2012), and whether the diurnally modulated convection is part of a large-scale organized system or not (Tripoli 1992; Sui et al. 1997; Kubota and Nitta 2001; Nesbitt and Zipser 2003; Cifelli et al. 2008). An excellent review of the proposed mechanisms involved in modulating the diurnal cycle over both land and oceans is presented by Yang and Smith (2006).

Understanding how these mechanisms influence convection is important for improving the representation of the diurnal cycle in regional and global models (Dai and Trenberth 2004; Wang et al. 2007) without the computational expense associated with super-parameterized (Pritchard and Somerville 2009) or global cloud resolving models (Sato et al. 2009; Noda et al. 2012). One approach to this problem is to consider the following question: To what extent is the diurnal convection over tropical oceans modulated by changes in the thermodynamic environment?

Raymond and Sessions (2007) showed that modeled convection in the context of the weak temperature gradient (WTG) approximation is sensitive to changes in the potential temperature and moisture profiles representing the convective environment. They found that both moister or more stable environments resulted in more extensive convection with higher average precipitation rates compared to unperturbed conditions. They also found that the more stable conditions produced more "bottom-heavy" convective mass flux profiles with higher precipitation efficiencies.

Wang et al. (2013) recently performed WTG simulations with time-dependent reference profiles generated from TOGA COARE (Tropical Ocean Global Atmosphere Program's Coupled Ocean Atmosphere Response Experiment) observations. Their results suggested that the observed precipitation variability was influenced more by forcing from surface fluxes than by changes in the potential temperature profiles. It is worth noting that their study excluded lateral entrainment of moisture from outside the model domain which may be important in WTG simulations.

The weak temperature gradient (WTG) approximation provides a unique tool for assessing the relative importance of the thermodynamic environment in the diurnal forcing of convection. The WTG approximation represents a parameterization of the large scale based on approximate horizontal homogeneity of virtual temperature in the tropical atmosphere. In WTG simulations, convection evolves to maintain a specified reference temperature which represents the convective environment. If a particular forcing mechanism diurnally modulates the thermodynamic environment in which the convection is evolving, and if the convection is sensitive to those changes, then the properties of WTG-simulated convection should exhibit observed characteristics of the diurnal variability in convection. Thus, we expect good representation of the observed characteristics if (1) the dominant diurnal forcing mechanism manifests in the thermodynamic profiles, and (2) if the convection is sufficiently sensitive to the thermodynamic environment.

Whether or not this approach is successful will provide valuable information for improving the representation of the diurnal cycle in global models. In particular, identifying the specific mechanisms may be unnecessary if it is sufficient to note that they act via the thermodynamic environment. This would greatly reduce the factors that need to be accounted for in large scale models, given the extreme space and time heterogeneity in the observed diurnal cycles over tropical oceans. On the other hand, if convection simulated via the WTG approximation fails to capture the diurnal variability, we can assume that the dominant mechanisms directly modulate the convection, and do not act through the thermodynamic environment.

To demonstrate the application of the WTG approximation in diurnal forcing, we incorporate observational data taken during the 2001 field program, EPIC2001 (East Pacific Investigation of Climate Processes in the Coupled Ocean-Atmosphere System; Raymond et al.

2004), into WTG simulations. In this region, it is believed that the dominant mechanism for diurnal variations is modulation by gravity waves initiated from land based convection (Cifelli et al. 2008; Mapes et al. 2003b; Takahashi 2012). This location is just within the range of this effect (see, e.g., Cifelli et al. 2008; Takahashi 2012); however, it doesn't preclude the influence of other mechanisms, including the dynamic radiation-convection effect (Ruprect and Gray 1976a,b; Gray and Jacobson 1977) which results from an oscillation between cloudy and adjacent cloud-free regions, or the static radiation-convection mechanism (Kraus 1963; Ramage 1971; Randall et al. 1991), in which the nighttime convection is enhanced by an increase in the radiative cooling of the cloud tops which thermally destabilizes the upper cloud. While it is clear that the gravity wave mechanism would act via the thermodynamic profiles, it is likely that these alternate mechanisms would also alter the potential temperature profiles and thus affect the development of convection. The goal of the present study is not to determine which of these is dominant, but rather to determine the extent to which changes in the thermodynamic profiles–regardless of how those changes occur–influence the diurnal modulation of convection over open oceans. While these mechanisms represent an explanation for the early morning precipitation maximum, some ocean regions also exhibit a weak afternoon peak which results from the heating of the ocean surface by solar insolation. Since an afternoon peak was not observed during the EPIC program (Cifelli et al. 2008; Raymond et al. 2004), this mechanism is likely to be insignificant for this work. Other mechanisms summarized in Yang and Smith (2006) cannot be distinguished in the work presented here, for reasons that we discuss in section 1b.

In the following sections, we briefly describe the observational data used for this study, as well as the essential ingredients for the particular implementation of WTG used in our cloud system resolving model. Following that, section 2 gives results from our simulations and compares those with corresponding observations. We discuss the significance of the results and conclude in section 3.

a. *Weak temperature gradient (WTG) approximation*

In this work, we use an updated version of the cloud system resolving model (CRM) described in Raymond and Zeng (2005). The model implements the weak temperature gradient approximation similar to that introduced by Sobel and Bretherton (2000). The basic idea is that buoyancy anomalies are rapidly redistributed throughout the tropical troposphere, resulting in a nearly horizontally homogeneous virtual temperature profile. In nature, this effect is achieved by gravity waves (Bretherton and Smolarkiewicz 1989; Mapes and Houze 1995). In the model, we accomplish this by generating a hypothetical vertical velocity, w_{wtg} (the weak temperature gradient vertical velocity), which counteracts the effects of diabatic heating. The WTG velocity obeys mass continuity independent of the velocity field in the model (see Raymond and Zeng 2005 or Sessions et al. 2010 for a thorough discussion of the implementation of WTG in the CRM).

The WTG vertical velocity enters in the governing equation for potential temperature, θ[1]:

$$\frac{\partial(\rho\theta)}{\partial t} + \nabla \cdot (\rho \mathbf{v}\theta + \mathbf{T}_\theta) \equiv \rho(S_\theta - E_\theta) \quad , \tag{1}$$

where ρ is the density, $\mathbf{v}$ is the wind field computed explicitly by the model (which does not include the contribution from enforcement of WTG), $\mathbf{T}_\theta$ is the contribution due to unresolved eddy and viscous transport, S_θ is the diabatic source of potential temperature, and E_θ enforces the WTG approximation via a relaxation of θ to a reference profile θ_0:

$$E_\theta = w_{wtg}\frac{\partial\overline{\theta}}{\partial z} = \sin(\pi z/h)\frac{\overline{\theta} - \theta_0(z)}{t_\theta} \quad . \tag{2}$$

Here, the overbar signifies a horizontal average over the model domain, h is the tropopause height, and t_θ is the time scale over which the domain averaged potential temperature profile relaxes to the reference profile. Practically speaking, t_θ is a measure of enforcement of WTG:

[1] The weak temperature gradient approximation really applies to horizontal homogeneity of the virtual temperature. Our model doesn't distinguish between virtual and potential temperature so we enforce WTG via the potential temperature budget.

$t_\theta \to 0$ corresponds to strict WTG enforcement (as implemented in Sobel and Bretherton 2000), while $t_\theta \to \infty$ turns WTG-mode off and allows the domain to evolve to radiative convective equilibrium (RCE). Physically, t_θ is believed to be associated with the time it takes gravity waves to travel some characteristic distance in the model. In the work presented here, we vary t_θ and examine its effect on the ability of the model to capture the diurnal cycle.

To examine the diurnal cycle, we prescribe time-dependent perturbations to the reference potential temperature profile, and we therefore modify the reference profile in equation (2) to be time-dependent, $\theta_0(z, t)$. This is similar to the approach used by Wang et al. (2013), who imposed the observed, time-dependent potential temperature profile from TOGA COARE in the enforcement of WTG. There are several significant differences between their work and the work presented here. The first is that they do not include a sinusoidal modulation of the potential temperature profile that is given in equation (2). This essentially represents a modulation of the gravity wave speed; the enforcement of WTG in our model is strongest in the mid-troposphere and attenuates toward the tropopause and boundary layer. Both here and in Wang et al. (2013), the enforcement of WTG in the boundary layer is linearly interpolated to zero at the surface, since WTG is not a good approximation in the boundary layer (Sobel and Bretherton 2000). Also, Wang et al. (2013) impose a relaxation time scale of 4 hours. This is not fast enough to allow the convection to respond to diurnal variations in the thermodynamic profiles, and thus we choose shorter relaxation times (see section 1c).

Probably the most significant difference between Wang et al. (2013) and the work presented here is the treatment of moisture. In both studies, moisture within the model domain is advected vertically by the WTG vertical velocity (w_{wtg} in equation (2)); however, Wang et al. (2013) do not in any way incorporate moisture outside the model domain into the computational domain. There are three choices for how to incorporate environmental moisture from outside the model domain into the domain. The first is via horizontal advection by large scale circulations. The second is by specifying a separate moisture relaxation time analogous to the potential temperature relaxation time given in equation (2). This was done in Sobel et al. (2007), and they found that relaxation to the reference profile has a significant impact on the ability of a model domain to sustain multiple equilibria[2]. Alternatively, we adopt a third method which was originally implemented in Raymond and Zeng (2005). In this case, moisture is entrained laterally into the model domain by satisfying mass continuity in the WTG velocity field. The governing equation for total water mixing ratio, r_t, is given by:

$$\frac{\partial(\rho r_t)}{\partial t} + \nabla \cdot (\rho \mathbf{v} r_t + \mathbf{T}_r) \equiv \rho(S_r - E_r) \quad , \tag{3}$$

with $\mathbf{T}_r$ the contribution from unresolved eddy and viscous transport, S_r the source of r_t due to precipitation and evaporation, and E_r represents both entrainment from the environment and vertical transport by large scale vertical motion:

$$E_r = \frac{(r_t - r_x)}{\overline{\rho}} \frac{\partial(\overline{\rho} w_{wtg})}{\partial z} + w_{wtg} \frac{\partial r_t}{\partial z} \quad . \tag{4}$$

Here,

$$r_x = \begin{cases} r_0(z,t) & \frac{\partial(\overline{\rho} w_{wtg})}{\partial z} > 0 \quad , \\ \overline{r_t} & \text{otherwise} \quad . \end{cases} \tag{5}$$

This definition ensures that outflowing air has a mixing ratio equal to the model domain while inflowing air has a mixing ratio equal to that of the reference profile, $r_0(z,t)$. In previous work, the reference moisture profile, r_0, was time-independent; here we generalize the definition in anticipation of the diurnal variability of moisture observed during EPIC.

Another difference between the general procedure described in Wang et al. (2013) and the method here is the treatment of radiation. In order to avoid complications arising from cloud-radiation feedbacks, they prescribe a non-interactive, time-dependent radiative heating profile obtained from a simulation with imposed vertical motion (their control simulation). Our model uses interactive radiation computed from a toy radiation model (Raymond and Zeng 2000) which cools uniformly across the domain.

[2]Here, multiple equilibria refers to the ability for a model domain to maintain both a dry or a precipitating steady state with identical boundary conditions but different initial conditions. See also Sessions et al. (2010).

Finally, it is interesting to note that the reference profiles from TOGA COARE used in Wang et al. (2013) represent profiles averaged over the entire Intensive Flux Array (IFA) region and the results are compared against the budget-derived precipitation rate for the IFA region. In the work described here, profiles are obtained from a source at a single location, and we compare precipitation rates with observations from radar aboard the ship.

An important ingredient in the implementation of WTG is specification of the reference profiles of potential temperature and mixing ratio (θ_0 and r_0, respectively). We usually take time and domain averages of a simulation run to radiative-convective equilibrium (i.e., $t_\theta \to \infty$ in equation (2)) to represent the environmental conditions outside the model domain. In this work, we add observed diurnal anomalies to the RCE reference profiles to investigate the response of modeled convection to diurnal variations in the temperature and moisture profiles. The observed anomalies were constructed from the EPIC2001 field program, which is described in the next section. Following that, we provide details of the model set-up and describe the parameter space investigated in this study.

b. EPIC2001 data

The focus of the EPIC field program was to document and understand the mechanisms of subseasonal variability in the East Pacific (see Raymond et al. 2004). The project lasted from September 1 to October 10, 2001. The scope of the project included observations of a deep layer of the atmosphere as well as upper layers of the ocean. The observations which contribute to this study were all obtained from ship-based measurements from NOAA's research vessel *Ron H. Brown* (RHB). During the field program, radiosondes were launched every four hours, which provide a time series of the thermodynamic environment at the ship location (95°W, 10°N). Rainfall measurements were estimated from the radar aboard the RHB, and are freely available from the CODIAC website (`http://data.eol.ucar.edu/codiac/`). We choose the Z-R relation for precipitation calibrated from insitu data taken from NCAR's C130 measurements for comparison with observations.

We use the observational data in two ways: (1) to construct diurnal perturbations for the reference profiles used in the WTG simulations, and (2) as a validation of model results. The latter is discussed in section 2. To construct the diurnal perturbations, we started with the time series taken from the JOSS/UCAR quality controlled soundings[3]. From these, we derived a time series of potential temperature and mixing ratio profiles. Each day is divided into four-hour time intervals, and each time interval is averaged over all days. In this way, we construct thermodynamic profiles of a "typical day". We note that during EPIC, several easterly waves passed by and were observed from the RHB (Petersen et al. 2003; Raymond et al. 2004). The process of constructing a "typical day" effectively averages out the thermodynamic conditions for the easterly waves, though these could contaminate the time series compared to observations in undisturbed conditions. Given that some diurnal cycle mechanisms operate differently in clear versus disturbed regions (Tripoli 1992; Sui et al. 1997; Nesbitt and Zipser 2003; Yang and Smith 2006; Cifelli et al. 2008), we have eliminated our ability to isolate these effects in the WTG approximation. Nevertheless, this stands as a first step toward understanding the role of the thermodynamics in the diurnal modulation of convection. For the purpose of this work, we linearly interpolate the profiles to a regular temporal grid with one-hour resolution.

Radiative convective equilibrium represents conditions in the model's native environment. Thus, rather than directly imposing the thermodynamic profiles observed in EPIC, we add the diurnal anomalies to the model's RCE profile (see figures 1 and 2). In order to construct statistically significant results, we repeat the simulation with diurnal anomalies for 25 consecutive days. For comparing the model results with observations, we keep data from days 5-25, and composite all of the days for the "typical model day" with 1 hour resolution.

[3] Soundings recorded measurements of dew point, relative humidity, temperature, pressure, and horizontal wind velocity with 2 s vertical resolution.

c. *Experimental setup*

In order to understand the diurnal cycle in the context of the weak temperature gradient approximation, it is important to note that the only diurnal modulation occurs in the reference potential temperature and moisture profiles. These are assumed to represent the conditions immediately outside the model domain. We impose no diurnal forcing in the surface fluxes or in radiative cooling. This is an important point given the results from Wang et al. (2013) which suggest that these are both important factors in modulating precipitation variability during TOGA COARE.

As mentioned in section 1a, we use a version of the model described in Raymond and Zeng (2000), which implements the WTG approximation. All simulations are run with 2-dimensional domains. The vertical dimension is 20 km, with a tropopause height of 15 km. The WTG approximation is enforced in the altitude range between 1 km and 15 km. The WTG vertical velocity is linearly interpolated to zero below 1 km. The vertical resolution is 250 m. The horizontal domain is doubly periodic and ranges in size from 100 to 400 km, with one kilometer resolution. Sessions et al. (2010) found that the existence of multiple equilibria in WTG simulations was sensitive to domain size, so we are investigating the extent to which domain size affects characteristics of convection with diurnally modulated reference profiles.

For each domain size used, we ran the model for 50 days in non-WTG mode to construct the RCE reference profile which serves as the baseline for diurnal anomalies. RCE was calculated for a surface wind speed of 5 m s^{-1} over an ocean with a sea surface temperature (SST) of 303 K. Figure 1 compares the RCE profiles of potential temperature and mixing ratio for the 200 km domain with the observed mean profiles. The differences between the observed and RCE profiles for all domain sizes are shown in figure 2. The model RCE states are 1-2 K warmer through most of the troposphere, but cooler above 10 km compared to observed conditions; they are dryer in the 2 km layer just above the boundary layer, and moister aloft. Also note that the 400 km domain has the largest differences from the observed potential temperature profile (differences between 100 and 200 km domains are negligible in figure 2a), while the 100 km domain is the driest in the mid-troposphere compared to the other RCE states and the observations. For this reason, we choose to perform most of our sensitivity experiments on a 200 km domain.

For each set of RCE reference profiles, we impose the diurnal anomalies derived from the EPIC field program. These are shown in figure 3 (local time, LT). Note that in the early morning hours (0000-0400 LT), the lowest 5 km are moist and cool relative to the daily mean. Both of these would be expected to produce heavier precipitation, according to results from Raymond and Sessions (2007). As the day progresses, the lower troposphere dries and becomes more unstable, which is expected to decrease precipitation efficiency. Based on the observed diurnal anomalies and the results from Raymond and Sessions (2007), we would expect the precipitation maximum to occur between 0-4 LT, with an afternoon minimum. Note the significant anomalies in potential temperature near the tropopause throughout most of the day. While the enforcement of the WTG approximation will certainly respond to those anomalies, the gravity waves enforcing WTG attenuate at altitudes approaching the tropopause as a result of the sinusoidal modulation in equation (2). While this helps damp the influence of these anomalies, we note that care should be taken in interpreting model results at high altitudes.

In order to procure a large enough sample for statistical averaging, we impose the diurnal anomalies shown in figure 3, linearly interpolated to every hour, for 25 consecutive simulation days. The model diurnal cycle is constructed from the average of each hour for the last 20 days of the 25 day simulations. In order to assess the variability in the model results, we run a few simulations for 45 days and compare averages from two different 20 day segments.

In addition to varying the domain size, we also considered the effect of additional constant surface fluxes by increasing the surface wind speed relative to RCE conditions. A diurnal cycle was not imposed in surface wind speed, SSTs, or in the radiation scheme (diurnal variations are imposed only in the reference profiles of potential temperature and mixing ratio). Though the increase in SST from solar insolation likely contributes to the minor afternoon peak (Chen and Houze 1997; Sui et al. 1997; Yang and Smith 2006), the afternoon peak is not observed in the EPIC region (Cifelli et al. 2008; Raymond et al. 2004). This mechanism also tends to be more prevalent in undisturbed or clear regions (Nesbitt and Zipser 2003; Cifelli et al. 2008), and the passing easterly waves during EPIC would have made it difficult to capture this effect. Furthermore, Cifelli et al. (2008) showed that the diurnal variability in latent heat flux, SST, and surface wind speed was small during EPIC. Thus, we justify the neglect of diurnal forcing in surface fluxes both because we expect this to be a small contribution to the diurnal cycle in precipitation, and because our primary goal is to determine the extent to which convection is forced by diurnal changes in the thermodynamic environment. Our results will be particularly interesting in light of the Wang et al. (2013) conclusions that the intraseasonal variability in TOGA COARE is largely a result of surface forcing.

Finally, we also investigate how the degree to which the WTG approximation is strictly enforced affects the model's ability to generate a diurnal cycle. To do this, we vary the potential temperature relaxation time, t_θ in equation (2). We do not expect to detect diurnal variations for large t_θ since the convection will respond on a time scale longer than the time scale of changes in the perturbations. As t_θ becomes smaller than the time scale of diurnal variability, the modeled convection responds much faster to those changes and we expect to generate a diurnal cycle with which we can compare to observations.

2. Results

Our primary goal is to compare the observed diurnal variability with simulations having diurnal forcing imposed in the thermodynamic environment and enforced via the WTG approximation. The most significant comparison is in the diurnal cycle of precipitation. For this, we use the median radar-derived rain rate over a domain which extends 100 km in all directions from the *Ron H. Brown*. The Z-R relation used is from the Baumgardner C-130 insitu data (Cifelli et al. 2002). We also use this data to compare the fraction of the model domain that is precipitating to the observed rain fraction.

In addition to precipitation rate and rain fraction, we compare several other variables which can easily be calculated from the sonde data used for the diurnal forcing in the WTG simulations. These include a measure of the atmospheric instability, saturation fraction, deep convective inhibition, the vertical distribution of moisture, and mean boundary layer mixing ratio.

Atmospheric instability is diagnosed from the saturated moist entropy. We define an instability index according to

$$\Delta s^* = s^*_{low} - s^*_{mid} \quad , \tag{6}$$

where s^*_{low} is the saturated moist entropy averaged over the 1-3 km layer and s^*_{mid} is the saturated moist entropy averaged over the 5-7 km layer. If the environment is saturated, larger Δs^* corresponds to greater instability which promotes higher precipitation rates, according to Raymond and Sessions (2007).

The saturation fraction is defined as the ratio of precipitable water to saturated precipitable water. As in Raymond et al. (2011), we approximate the moist entropy by $s \approx s_d + Lr_v/T_R$, where s_d is the dry entropy, L is the (constant) latent heat of condensation, r_v is the water vapor mixing ratio, and T_R is a constant reference temperature. Using this, we can approximate the saturation fraction by

$$S \approx \frac{\int_0^h \rho(s - s_d)dz}{\int_0^h \rho(s^* - s_d)dz} \quad , \tag{7}$$

where the integrals are taken from the surface to the tropopause height, h.

We also compare the deep convective inhibition (DCIN; Raymond et al. 2003), which is defined as

$$DCIN = s^*_t - s_b \quad , \tag{8}$$

where s^*_t is the vertical average of saturated moist entropy over the height range 2000-2500 m; it is the threshold entropy for convection. The boundary layer entropy, s_b, is defined as the vertical average of moist entropy over the height range 0-1750 m.

Cifelli et al. (2008) showed that diurnal variability in the mean boundary layer mixing ratio also exhibited a significant diurnal amplitude. Given that our model does not adequately resolve the boundary layer, and that WTG does not apply in this layer, we would not expect good agreement with observations. Nevertheless, we calculate the mean boundary layer mixing ratio in the lowest kilometer and compare with observations.

Nesbitt and Zipser (2003) and Biasutti et al. (2012) analyzed satellite data and concluded that the diurnal cycle in this region is a result of more frequent convective events rather than more intense events. This is consistent with the Cifelli et al. (2008) observation that there is a diurnal cycle in the fraction of the region that is precipitating (rain fraction). To see if our model qualitatively captures these observations, we compare the fraction of the model domain which is precipitating to the reported fractional area of precipitation in Cifelli et al. (2008). For this purpose, a grid point is considered precipitating if it has a precipitation rate of at least 1 mm hour^{-1}.

We begin the data analysis with a comparison between observations and the results from selected WTG simulations.

a. Comparison with EPIC observations

In comparing the WTG simulations with observations, we would expect the best results with a strict enforcement of WTG. Figure 4 compares the observed values of rain rate, instability index, saturation fraction, DCIN, mean boundary layer mixing ratio, and rain fraction to select WTG simulations. The simulations shown correspond to strict enforcement of WTG ($t_\theta = 6.7$ s in equation (2), which just larger than the 5 second time step implemented in the model) on 100, 200, and 400 km domains, and a slightly relaxed enforcement ($t_\theta = 67$ s) of the WTG approximation on a 200 km domain.

Not all observed features in the diurnal variability are reproduced in the WTG simulations; however, the model does an excellent job in capturing the early morning precipitation peak with a mid-afternoon/early-evening minimum. The 200 km domain with strict enforcement of WTG (black short-dashed line in figure 4a) shows an earlier peak at 0400 LT compared to the EPIC observations or the other two simulations shown. However, the exact timing and magnitude of the early morning peak is quite variable, even within a single model run. Figure 5 shows a comparison between two different 20 day segments in the 45 day run for the 200 and 400 km domains with strict enforcement of WTG. The saturation fraction and instability index exhibit no change in the timing of the diurnal variations, while the timing of the precipitation maximum varies up to 3 hours. Similar variability is exhibited with a 100 km domain (not shown). While this figure provides a sense of the magnitude of the noise in these simulations, it nevertheless maintains a clear diurnal cycle which agrees well with observations.

All simulations in figures 4 and 5 show considerably reduced precipitation rates in the afternoon compared to observations. One may hypothesize that this is a result of excluding the diurnal variability in surface fluxes which result from SST and wind speed variability. We do not think this is the case here because the diurnal variability in these quantities so small (0.5 K and 0.7 m s^{-1}, resp. Cifelli et al. 2008) that they are insufficient to increase the precipitation rate by 5 mm day^{-1} in our model (compare precipitation rates for wind speeds of 5 and 10 m s^{-1} in figure 8). Instead, we suspect that the dramatic reduction in precipitation rate in the late afternoon compared to the peak value in early morning is more likely a result of the two-dimensionality in the model domains. Wang and Sobel (2011) compared WTG simulations between two- and three-dimensional (2D and 3D, respectively) CRM domains. They found that 2D domains had lower values of gross moist stability (GMS) which resulted in larger precipitation rates compared to corresponding 3D runs. Raymond and Sessions (2007) demonstrated that lower GMS is associated with increased stability, so we interpret these results as an enhancement of the precipitation response to instability via GMS in 2D compared to 3D (Wang and Sobel 2011). This effect also seems to apply to smaller domain sizes (see figure 4 and section 2c). Thus, a more stable atmosphere would produce more precipitation while a more unstable atmosphere would correspond to smaller precipitation rates with the effect exaggerated in 2D.

The WTG simulations in general do an excellent job of capturing the diurnal variability in atmospheric instability and DCIN (figures 4b,d). This is perhaps not surprising since the simulations shown represent strict enforcements of the WTG approximation, which means that we expect potential temperature anomalies in the model to replicate observed diurnal anomalies (this is the forcing imposed after all). Figure 6 shows excellent agreement between the observed diurnal anomalies in potential temperature from the EPIC soundings and from the strict enforcement (i.e., $t_\theta = 6.7$ s) of WTG on the 400 km domain. Since DCIN is calculated from the entropy profiles (which are related to potential temperature), we expect these to follow the observed diurnal tendencies, and figure 4d shows this is indeed the case. Note that there is an offset between the observed and simulated instability index and DCIN. This is likely due to the differences in the mean thermodynamic profiles in the model environment compared to the real environment.

The most significant difference between the model and observed values occurs with the saturation fraction, as shown in figure 4c. In this case, the model captures the general trend, with the highest simulated values near the highest observed values, but it underestimates the saturation fraction in the early morning hours, and does not capture the late afternoon increase at all. We can understand these differences by comparing the vertical distributions of moisture in the model with those from the EPIC observations. The left panel of figure 7 shows the diurnal mixing ratio anomalies from the RHB soundings. These were added to the reference profile to represent the environmental moisture surrounding the model domain (r_0 in equation (5)). The right panel of figure (7) shows the diurnal variations in mixing ratio calculated by the model. While the model captures the timing in the diurnal variability, all of the variability is in the lowest few kilometers of the model domain; it completely misses the variations in the free troposphere. The lack of a positive moisture anomaly in the 1-5 km layer in the early morning explains the model's underestimation of the saturation fraction at this time. Similarly, the dry anomaly in the lowest model layer extends later in the afternoon than in observations, which explains in part why the afternoon peak is not seen in the model. A thorough analysis of the how the model is distributing moisture in the troposphere will be investigated in future work.

Despite the limitations of the model to accurately reproduce the free tropospheric moisture, the diurnal cycle in boundary layer moisture seems to qualitatively agree with observations. We can see that in the lowest layers in the mixing ratio shown in figure 7, and in the mean boundary layer mixing ratio shown in figure 4e. The latter also approximately agrees with the results in figure 5 of Cifelli et al. (2008).

Analysis of three years (1997-2000) of TRMM satellite data by Nesbitt and Zipser (2003) found that the peak in diurnal rainfall variability was almost exclusively a result of an increase in the number of systems, not in the intensity of the systems. A very high resolution analysis of the TRMM data between 1998 and 2007 by Biasutti et al. (2012) also attributed the peak in diurnal variability to an increase in frequency of rainfall, not intensity. As a quick check to see if the WTG simulations capture this tendency, we can look at the diurnal variability in rain fraction in the model domain. We define the rain fraction to be the fraction of the domain having a rainfall rate greater than 1 mm hr^{-1}. Figure 4f compares the rain fraction in the WTG simulations to the rain fraction observed during EPIC. The rain fraction increases proportionally to the rainfall, which indicates there is a larger fraction of the domain that is precipitating, rather than the same fraction with a higher intensity. This is qualitatively consistent with observations by Nesbitt and Zipser (2003) and Biasutti et al. (2012) and also agrees with the diurnal variability in rain area of mesoscale convective systems reported by Cifelli et al. (2008, see their figure 12), and simulated on a global CRM (Noda et al. 2012). Furthermore, it is notable that the rain fraction data derived from radar is independent of the sounding data used in the WTG simulations. Thus, it provides additional validation for investigating the diurnal variability in the context of the WTG approximation.

The results in this section are actually quite remarkable, and they suggest that enforcing the WTG approximation on diurnal timescales reproduces observed variability to a much better degree than might be expected. Though it is not surprising that the model reproduces the potential temperature variability and by extension the instability and DCIN, is it surprising that it gets the approximate timing in precipitation maximum correct, and it does a decent job on mean boundary layer mixing ratio and rain fraction. The main deficiency is that the model fails to capture the variability in the vertical profiles of moisture, and consequently some features in the saturation fraction. Despite this, the model still does a good job in representing the diurnal variability in the precipitation rate.

b. Sensitivity to WTG relaxation time

Here, we examine the sensitivity of the modeled diurnal cycle on the WTG relaxation time, t_θ, in equation (2). These experiments are performed using a 200 km domain, with surface wind speeds equal to the RCE wind speed ($v_y = 5$ m s^{-1}) to see the effect of diurnal variations in reference profiles only. We repeat these experiments with stronger surface wind speeds ($v_y = 10$ m s^{-1}) to examine the extent to which surface fluxes enhance or diminish the diurnal variability. Figure 8 shows the modeled diurnal cycle in precipitation rate, saturation fraction and instability index for the different relaxation time scales for surface wind speeds of 5 m s^{-1} (left panels) and 10 m s^{-1} (right panels). Observed values are shown in blue.

As seen in figure 8, the diurnal amplitude diminishes rapidly with even a slight increase in the relaxation time scale. It is virtually absent in all observables for $t_\theta \geq 1$ hour, though prominent features are all retained for $t_\theta \sim 10$ minutes, regardless of the the imposed surfaces fluxes (which are modulated by a constant surface wind speed in this case). The reason that the diurnal variability vanishes for longer relaxation times is because the reference profile is changing faster than the model has time to adjust to those changes. This suggests that convection must respond rapidly to diurnal variations in the thermodynamic environment for this to be a viable mechanism in the diurnal cycle.

Increasing the imposed wind speed, and hence surface fluxes, enhances the diurnal cycle in precipitation for strict enforcement of WTG ($t_\theta \leq 11$ minutes). The additional moisture (comparing middle panels in figure 8) in the early morning hours contributes to the larger precipitation maximum in the early morning as well as a slight increase in the afternoon precipitation rate compared to lower surface wind speeds. The dramatic increase in precipitation rate in the early morning hours compared to the slight increase in the late afternoon for a proportional increase in saturation fraction is likely a result of the sensitive dependence of precipitation rate on saturation fraction (Bretherton et al. 2004; Raymond et al. 2007) as well as the increase in precipitation efficiency due to a more stable environment (Raymond and Sessions 2007).

Examining the instability index in these experiments is a simple way to diagnose the enforcement of WTG. It explains why the diurnal variability based on forcing via the thermodynamic profiles vanishes with a weaker enforcement of WTG. Once the diurnal cycle in the instability index vanishes, the lateral entrainment of environmental moisture becomes uniform and the diurnal signal vanishes in both saturation fraction and precipitation rate.

c. *Effect of domain size*

Figure 4 shows the effect of domain sizes varying from 100 km - 400 km on the model's ability to reproduce the observed diurnal variations. With strict enforcement of WTG, the instability index closely resembles the observed values for all domain sizes. There are slightly lower values for the 400 km domain compared to the 100 and 200 km domains, which is a result of the slightly warmer free troposphere in RCE for the 400 km domain compared to the other two (see figure 2). Also, we can see that the smaller the domain, the higher the mean saturation fraction, which is also a result of the moister free troposphere for successively smaller domains in the unperturbed RCE profiles (figure 2). It is interesting to see how these variations affect the domain mean precipitation rates for the different domain sizes. Probably the most significant difference is the magnitude of precipitation rate in the 100 km domain compared to the 200 and 400 km domains. The peak precipitation rate for the

100 km domain is 60 mm day^{-1} (peak not shown) near 0300 LT, whereas the peak rates for the 200 and 400 km domains are much closer to the observed 16 mm day^{-1}. This is likely a result of a combination of the moister reference environment and the exaggerated increase in precipitation efficiency for more stable environments (see the discussion in section 2a).

3. Discussion and conclusions

The goal of this work is to determine to what extent the diurnal variability in convection over open oceans is modulated by changes in the thermodynamic environment. We performed a series of numerical experiments which incorporated diurnal anomalies observed in the vertical profiles of potential temperature and mixing ratio taken from radiosonde data during the EPIC2001 field program. The limited domain simulations implemented the weak temperature gradient approximation, which parameterizes the large scale environment by enforcing the potential temperature profile in the model to relax to the reference profile representing the environment outside the model domain. This enforcement generates a vertical velocity (the weak temperature gradient vertical velocity), which vertically advects moisture and, via mass continuity, results in lateral entrainment of moisture from the environment outside the domain.

There are several proposed mechanisms which explain the diurnal variability in precipitation over open oceans, and in particular the early morning rainfall peak. The EPIC region is just within the boundaries where gravity waves from land-based convection can modulate the convection, and this is believed to be an important mechanism in this location. Other potential mechanisms may be classified as interactions between radiation and convection, as explained in section 1. The work presented here does not aim to determine which of the possible mechanisms are responsible, only whether or not the convection responds sufficiently fast to changes in the thermodynamic environment so that the principal features in diurnal variability are reproduced in WTG simulations. Thus, we expect good results if (1) the mechanisms governing the diurnal variability manifest in the thermodynamic environment, and (2) if the convection is sufficiently sensitive to the thermodynamic environment. While not all of the proposed mechanisms would be expected to manifest in the thermodynamic environment (see Yang and Smith 2006), it is likely that the greatest contributions are from those that do (propagating gravity waves and radiation-convection interactions would certainly modify the local temperature profiles).

In order to assess the success of this approach, we compared the modeled diurnal variability in several observable quantities with measurements from the EPIC field program. While most of the comparisons were able to reproduce the general trends in the daily cycle, this might be expected by the design of the project. In particular, we imposed diurnal variations from the thermodynamic profiles taken from radiosonde measurements, and a significant number of our comparisons were against variables also measured in the soundings. Thus, the most significant comparison is between the model results and a source that is independent of the sounding data. For this purpose we use the radar-derived precipitation rate and rain fraction. With a strong enough enforcement of WTG, our model reproduces the observed early morning precipitation maximum and the corresponding peak in rain fraction. The diurnal variability in rain fraction indicates that a larger fraction of the model domain is precipitating rather than the same fraction with a higher intensity, consistent with observations. In this case, the modeled diurnal variations in precipitation are much stronger than observed, though they vanish as the enforcement of the WTG approximation weakens (i.e., as the potential temperature relaxation time scale approaches the time scale of the imposed changes, about 1 hour).

There are at least two significant results from this work. The first is, based on the ability of the model to reproduce significant features in the diurnal variability of convection over open oceans, we conclude that the diurnal variability is largely modulated by changes in the thermodynamic environment. The second is that WTG is a valid approach to understanding mechanisms controlling tropical convection. Wang et al. (2013) demonstrated one way to incorporate observations into WTG simulations to investigate dominant mechanisms in the evolution of the Madden Julian Observation. This work represents another example of incorporating observations to investigate a phenomenon on a completely different time scale and under different environmental conditions. The general idea of integrating observations in WTG simulations is a promising opportunity to make significant gains not only in our understanding of the convective response to changes in the environment, but to help identify mechanisms which dominate the convective evolution in a variety of different atmospheric conditions.

Acknowledgments.

We would like to thank Shuguang Wang and Adam Sobel for useful discussions, and Paquita Zuidema and Robert Cifelli for assistance with EPIC data, which is provided by NCAR/EOL under sponsorship of the National Science Foundation (`http://data.eol.ucar.edu/`). Many of the simulations were performed on The New Mexico Computing Applications Center supercomputer, ENCANTO, and on the supercomputer EXEMPLAR, located on the New Mexico Tech campus. This work was supported by U. S. National Science Foundation Grants AGS-1056254 and AGS-1021049.

REFERENCES

Biasutti, M., S. E. Yuter, C. D. Burleyson, and A. H. Sobel, 2012: Very high resolution rainfall patterns measured by TRMM precipitation radar: seasonal and diurnal cycles. *Climate Dyn.*, **39**, 239–258, doi:10.1007/s00382-011-1146-6.

Bretherton, C. S. and P. K. Smolarkiewicz, 1989: Gravity waves, compensating subsidence and detrainment around cumulus clouds. *J. Atmos. Sci.*, **46**, 740–759.

Bretherton, C. S., et al., 2004: The EPIC 2001 stratocumulus study. *Bull. Am. Meteor. Soc.*, **85**, 967–977.

Chen, S. S. and R. A. Houze, 1997: Diurnal variation and life-cycle of deep convective systems over the tropical Pacific warm pool. *Q. J. Roy. Meteor. Soc.*, **123**, 357–388.

Cifelli, R., D. Baumgardner, W. A. Petersen, S. A. Rutledge, C. Williams, P. Johnston, and K. Gage, 2002: Comparison Z-R relationships in EPIC-2001. *Eos Trans. AGU Fall Meet. Suppl.*, San Francisco, CA, AGU, Vol. 83(47), Abstract A22A–0053.

Cifelli, R., S. W. Nesbitt, S. A. Rutledge, W. A. Petersen, and S. Yuter, 2008: Diurnal characteristics of precipitation features over the tropical east Pacific: A comparison of the EPIC and TEPPS regions. *J. Climate*, **21**, 4068–4085, doi:10.1175/2007JCLI2020.1.

Dai, A. and K. E. Trenberth, 2004: The diurnal cycle and its depiction in the Community Climate System Model. *J. Climate*, **17**, 930–951.

Gille, S. T., S. G. L. Smith, and S. M. Lee, 2003: Measuring the sea breeze from Quikscat scatterometry. *Geophys. Res. Lett.*, **30**, 1114, doi:10.1029/2002GL016230.

Gray, W. M. and R. W. Jacobson, 1977: Diurnal variation of deep cumulus convection. *Mon. Wea. Rev.*, **105**, 1171–1188.

Hendon, H. H. and K. Woodberry, 1993: The diurnal cycle of tropical convection. *J. Geophys. Res.*, **98**, 16 623–16 637.

Jiang, Q., 2012: On offshore propagating diurnal waves. *J. Atmos. Sci.*, **69**, 1562–1581, doi:10.1175/JAS-D-11-0220.1.

Kraus, E. B., 1963: The diurnal precipitation change over the sea. *J. Atmos. Sci.*, **20**, 546–551.

Kubota, H. and T. Nitta, 2001: Diurnal variations of tropical convection observed during the TOGA-COARE. *J. Meteor. Soc. Japan*, **79**, 815–830.

Liu, C. and M. W. Moncrieff, 1998: A numerical study of the diurnal cycle of tropical oceanic convection. *J. Atmos. Sci.*, **55**, 2329–2344.

Mapes, B. E. and R. A. Houze, 1995: Diabatic divergence profiles in western Pacific mesoscale convective systems. *J. Atmos. Sci.*, **52**, 1807–1828.

Mapes, B. E., T. T. Warner, and M. Xu, 2003a: Diurnal patterns of rainfall in northwestern South America. Part I: Observations and context. *Mon. Wea. Rev.*, **131**, 799–812.

Mapes, B. E., T. T. Warner, and M. Xu, 2003b: Diurnal patterns of rainfall in northwestern South America. Part III: Diurnal gravity waves and nocturnal convection offshore. *Mon. Wea. Rev.*, **131**, 830–844.

Nesbitt, S. W. and E. J. Zipser, 2003: The diurnal cycle of rainfall and convective intensity according to three years of TRMM measurements. *J. Climate*, **16**, 1456–1475.

Noda, A. T., K. Oouchi, M. Satoh, and H. Tomita, 2012: Quantitative assessment of diurnal variation of tropical convection simulated by a global nonhydrostatic model without cumulus parameterization. *J. Climate*, **25**, 5119–5134, doi:10.1175/JCLI-D-11-00295.1.

Pereira, L. G. and S. A. Rutledge, 2006: Diurnal cycle of shallow and deep convection for a tropical land and an ocean environment and its relationship to synoptic wind regimes. *Mon. Wea. Rev.*, **134**, 2688–2701.

Petersen, W. A., R. Cifelli, D. J. Boccippio, S. A. Rutledge, and C. Fairall, 2003: Convection and easterly wave structures observed in the eastern Pacific warm pool during EPIC-2001. *J. Atmos. Sci.*, **60**, 1754–1773.

Pritchard, M. S. and R. C. J. Somerville, 2009: Assessing the diurnal cycle of precipitation in a multi-scale climate model. *J. Adv. Model. Earth Syst.*, **1**, 12, doi:10.3894/JAMES.2009.1.12.

Ramage, C. S., 1971: *Monsoon Meteorology*. Academic Press, 295 pp.

Randall, D. A., Harshvardhan, and D. A. Dazlich, 1991: Diurnal variability of the hydrologic cycle in a general circulation model. *J. Atmos. Sci.*, **48**, 40–62.

Raymond, D. J., G. B. Raga, C. S. Bretherton, J. Molinari, C. López-Carrillo, and Ž. Fuchs, 2003: Convective forcing in the intertropical convergence zone of the eastern Pacific. *J. Atmos. Sci.*, **60**, 2064–2082.

Raymond, D. J. and S. L. Sessions, 2007: Evolution of convection during tropical cyclogenesis. *Geophys. Res. Lett.*, **34**, L06 811, doi:10.1029/2006GL028607.

Raymond, D. J., S. L. Sessions, and C. L. Carrillo, 2011: Thermodynamics of tropical cyclogenesis in the northwest Pacific. *J. Geophys. Res.*, **116**, D18 101, doi:10.1029:2011JD015624.

Raymond, D. J., S. L. Sessions, and Z. Fuchs, 2007: A theory for the spinup of tropical depressions. *Q. J. Roy. Meteor. Soc.*, **133**, 1743–1754.

Raymond, D. J. and X. Zeng, 2000: Instability and large scale circulations in a two-column model of the tropical troposphere. *Quart. J. Roy. Meteor. Soc.*, **126**, 3117–3135.

Raymond, D. J. and X. Zeng, 2005: Modelling tropical atmospheric convection in the context of the weak temperature gradient approximation. *Quart. J. Roy. Meteor. Soc.*, **131**, 1301–1320.

Raymond, D. J., et al., 2004: EPIC2001 and the coupled ocean-atmosphere system of the tropical east Pacific. *Bull. Amer. Meteor. Soc.*, **85**, 1341–1354.

Ruprect, E. and W. M. Gray, 1976a: Analysis of satellite-observed cloud clusters. Part I: Wind and dynamic fields. *Tellus*, **28**, 391–413.

Ruprect, E. and W. M. Gray, 1976b: Analysis of satellite-observed cloud clusters. Part II: Thermal, moisture and precipitation. *Tellus*, **28**, 414–426.

Sato, T., H. Miura, M. Satoh, Y. N. Takayabu, and Y. Wang, 2009: Diurnal cycle of precipitation in the tropics simulated in a global cloud-resolving model. *J. Climate*, **22**, 4809–4826, doi:10.1175/2009JCLI2890.1.

Sessions, S. L., S. Sugaya, D. J. Raymond, and A. H. Sobel, 2010: Multiple equilibria in a cloud resolving model using the weak temperature gradient approximation. *J. Geophys. Res.*, **115**, D12 110, doi:10.1029/2009JD013376.

Sobel, A. H., G. Bellon, and J. Bacmeister, 2007: Multiple equilibria in a single-column model of the tropical atmosphere. *Geophys. Res. Lett.*, **34**, L22 804, doi:10.1029/2007GL031320.

Sobel, A. H. and C. S. Bretherton, 2000: Modeling tropical precipitation in a single column. *J. Climate*, **13**, 4378–4392.

Sui, C.-H., K.-M. Lau, Y. N. Takayabu, and D. A. Short, 1997: Diurnal variations in tropical oceanic cumulus convection during TOGA COARE. *J. Atmos. Sci.*, **54**, 639–655.

Takahashi, K., 2012: Thermotidal and land-heating forcing of the diurnal cycle of oceanic surface winds in the eastern tropical Pacific. *Geophys. Research Lett.*, **39**, L04 805, doi: 10.1029/2011GL050692.

Tripoli, G. J., 1992: An explicit three-dimensional nonhydrostatic simulation of a tropical cyclone. *Meteor. Atmos. Phys.*, **49**, 229–254.

Wang, S. and A. H. Sobel, 2011: Response of convection to relative sea surface temperature: cloud-resolving simulations in two and three dimensions. *J. Geophys. Res.*, **116**, D11 119, doi:10.1029/2010JD015347.

Wang, S., A. H. Sobel, and Z. Kuang, 2013: Cloud-resolving simulation of TOGA-COARE using parameterized large scale dynamics. *J. Geophys. Res.*, submitted.

Wang, Y., L. Zhou, and K. Hamilton, 2007: Effect of convective entrainment/detrainment of the simulation of the tropical precipitation diurnal cycle. *Mon. Wea. Rev.*, **135**, 567–585, doi:10.1175/MWR3308.1.

Warner, T. T., B. E. Mapes, and M. Xu, 2003: Diurnal patterns of rainfall in northwestern South America, Part II: Model simulations. *Mon. Wea. Rev.*, **131**, 813–829.

Yang, G.-Y. and J. Slingo, 2001: The diurnal cycle in the tropics. *Mon. Wea. Rev.*, **129**, 784–801.

Yang, S. and E. A. Smith, 2006: Mechanisms for diurnal variability of global tropical rainfall observed from TRMM. *J. Climate*, **19**, 5190–5226.

List of Figures

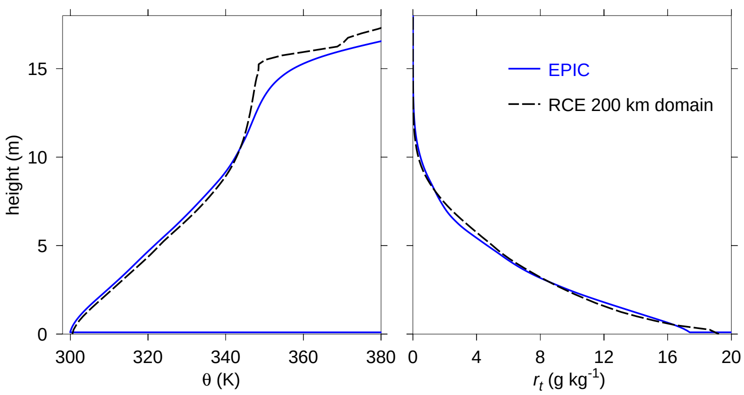

FIG. 1. Time-mean potential temperature (left) and mixing ratio (right) profiles. The blue lines are the observed profiles from EPIC, dashed black lines are RCE profiles on a 200 km domain. The RCE profiles are the unperturbed reference profiles for the WTG simulations.

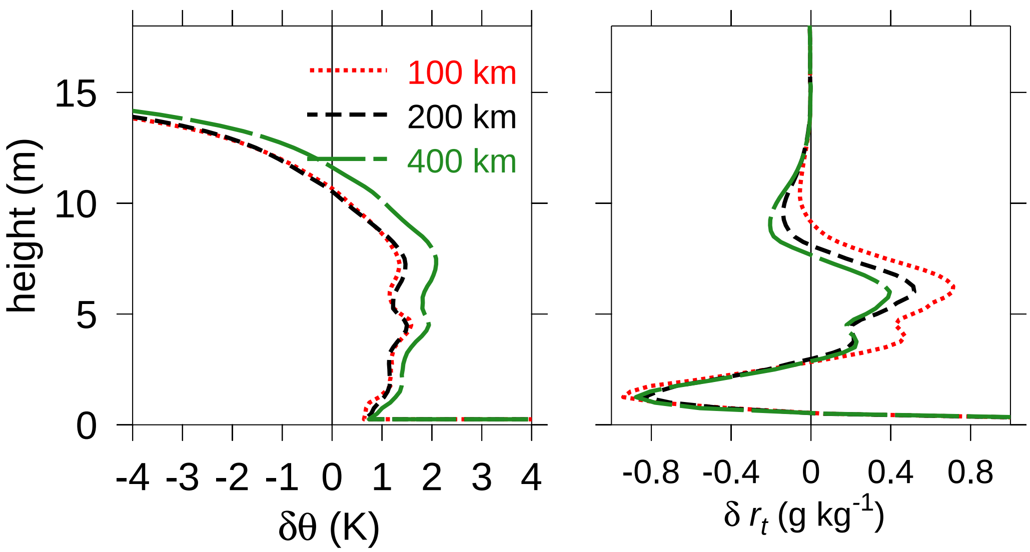

FIG. 2. Deviation of the RCE reference profiles from mean observations for domain sizes of 100, 200, and 400 km. For all domain sizes, the RCE profiles are 1-2 K warmer through most of the troposphere compared to observed conditions. The RCE profiles were also moister aloft and drier in the 2 km layer just above the boundary layer.

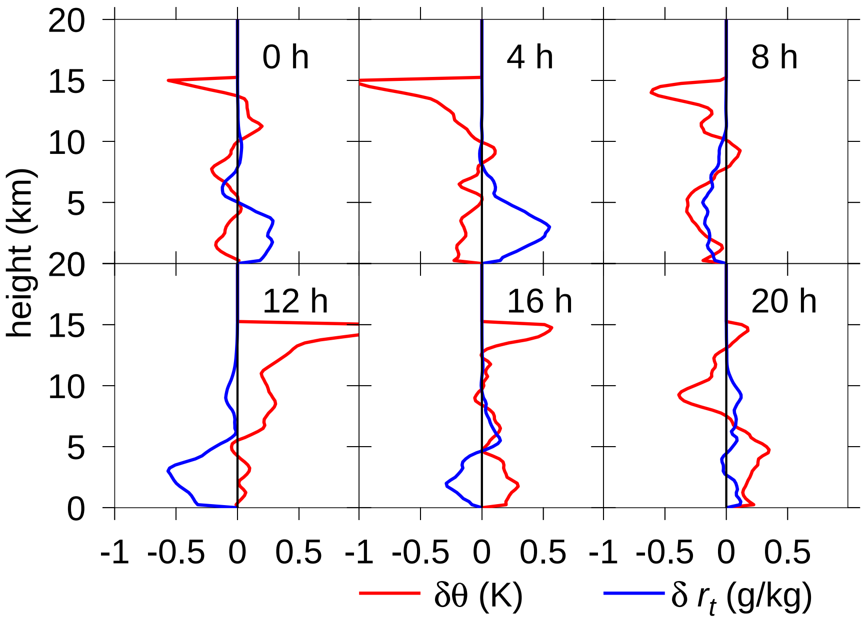

FIG. 3. Observed mean diurnal anomalies in potential temperature (red) and mixing ratio (blue). Hours shown are in local time (LT).

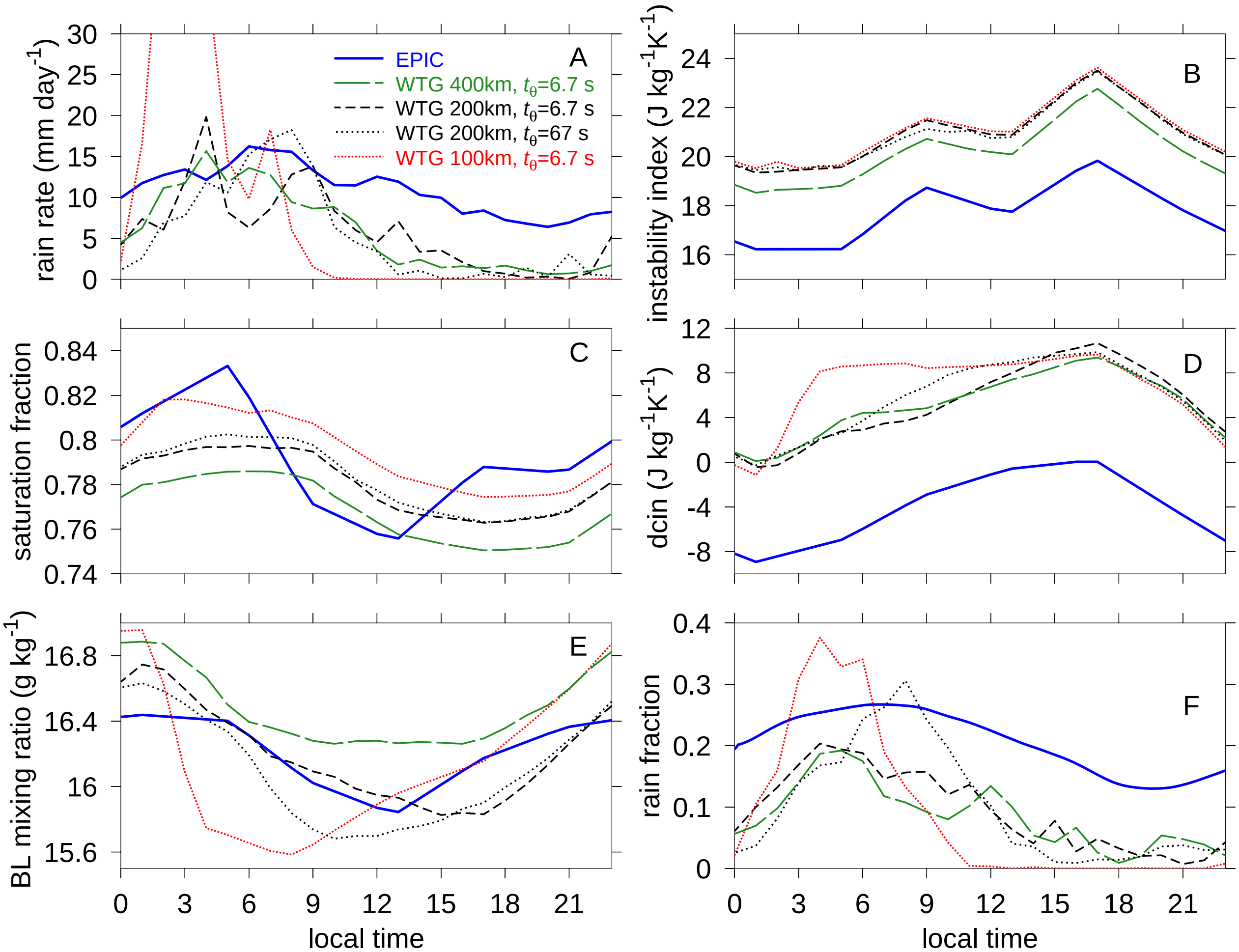

FIG. 4. Comparison between simulated diurnal cycle WTG simulations and observations: (A) precipitation rate, (B) instability index, (C) saturation fraction, (D) DCIN, (E) mean boundary layer mixing ratio, and (F) the fraction of the domain having a precipitation rate of at least 1 mm hour^{-1}. The solid blue line denotes observations from EPIC, the black dashed lines are from 200 km domains (short dashes for $t_\theta = 6.7$ s; long dashes for $t_\theta = 67$ s), the gray line is for the 400 km domain with $t_\theta = 6.7$ s.

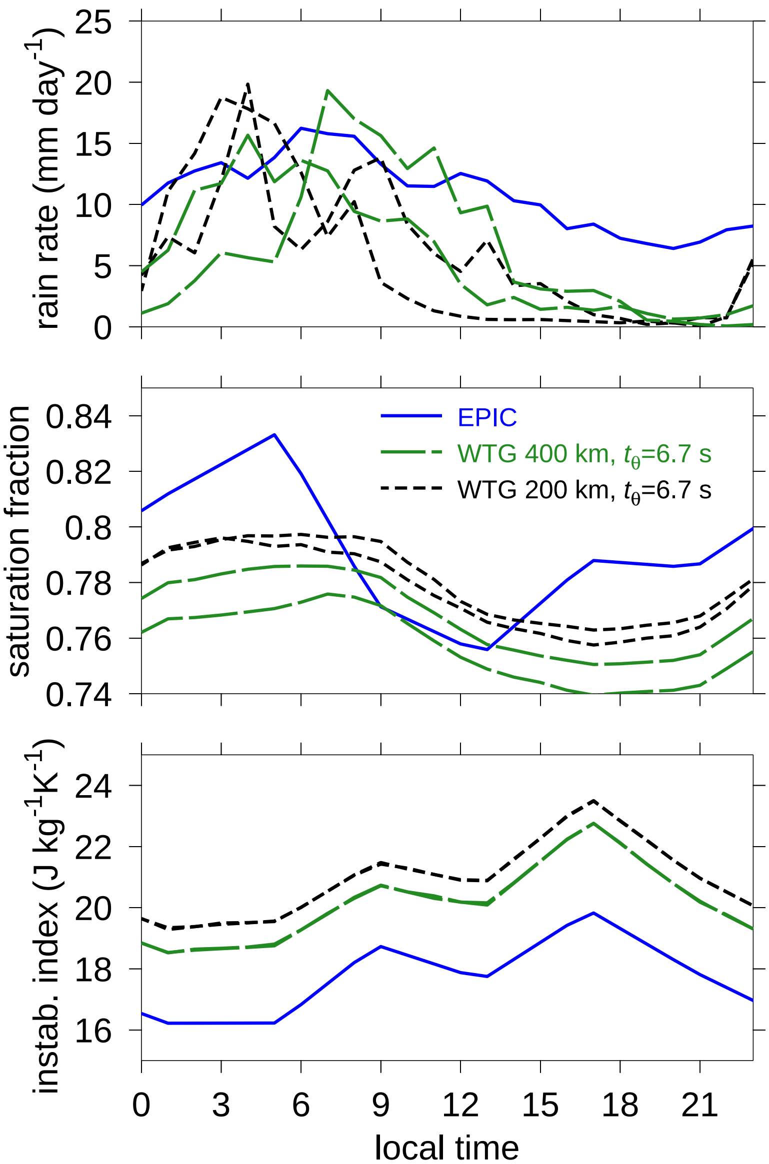

FIG. 5. Comparison between simulated diurnal cycle for composites of two different 20 day segments in single simulations with strict enforcement of WTG. Black short dashed lines and green long dashed lines are from 200 km and 400 km domains, respectively.

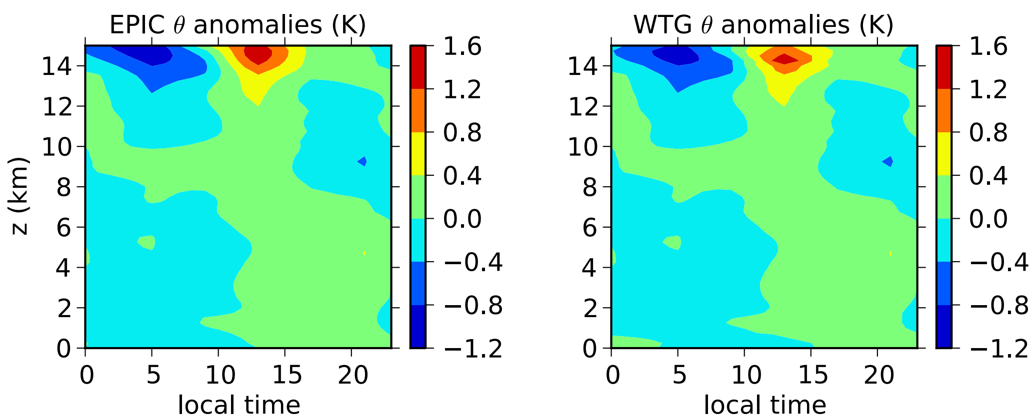

FIG. 6. The left panel shows the diurnal anomalies in potential temperature from the EPIC soundings. These were imposed in the reference profiles for the WTG simulations. The right panel shows the simulated potential temperature anomalies for a strict enforcement of WTG (i.e., $t_\theta = 6.7$ s) on a 400 km domain.

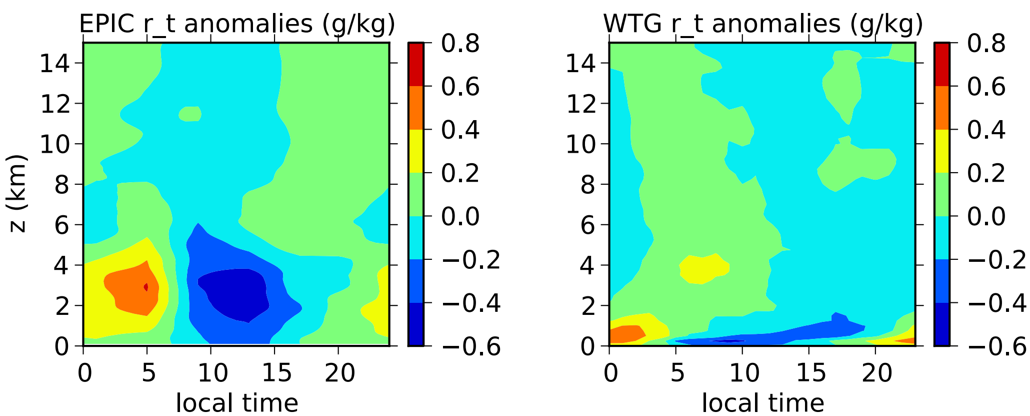

FIG. 7. The left panel shows the diurnal anomalies in mixing ratio from the EPIC soundings. These are the anomalies applied to $r_0(z,t)$ in equation 5 for the WTG simulations. The right panel shows the simulated mixing ratio anomalies for a strict enforcement of WTG (i.e., $t_\theta = 6.7$ s) on a 400 km domain.

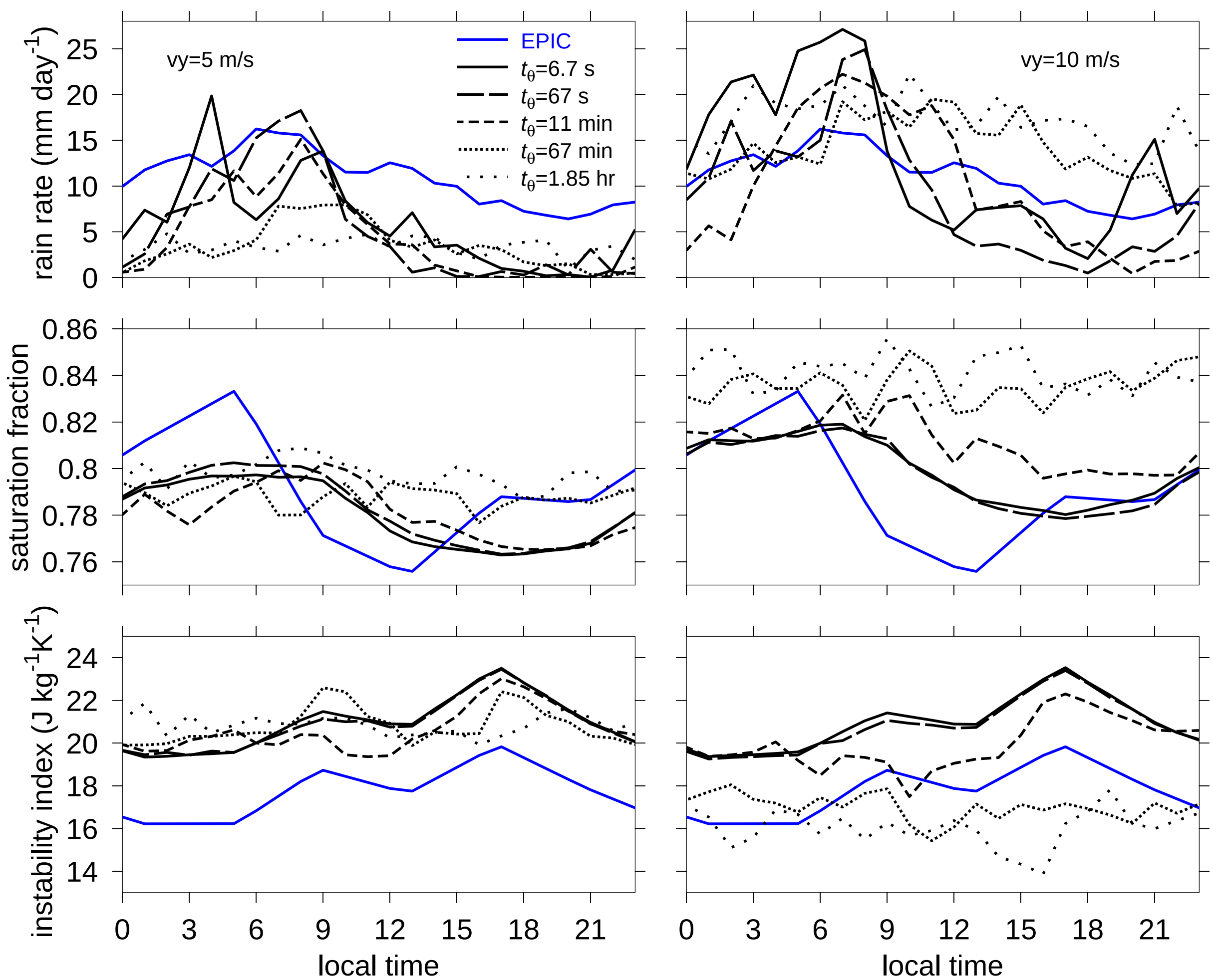

Fig. 8. Simulated diurnal cycle in precipitation rate (top), saturation fraction (middle), and instability index (bottom) for relaxation time scales ranging from 6.7 seconds to 1.85 hours. The left panels correspond to imposed surface wind speed of 5 m s^{-1}; the right panels have imposed surface wind speed of 10 m s^{-1}. Observed values from the RHB are shown in blue for comparison.